

Warm northern tropical Indian Ocean strengthened the ocean circulation prior to the last glacial termination

D. P. Singh^{1*ψ}, R. Saraswat^{1#}, M. Mohtadi², P. Kumar³

1. Micropaleontology Laboratory, CSIR-National Institute of Oceanography, Goa, India
 2. MARUM-Center for Marine Environmental Sciences, University of Bremen, Bremen, Germany
 3. AMS and Geochronology Division, Inter-University Accelerator Centre, New Delhi, India
- (For Correspondence: *dharmendra.singh@es.iitr.ac.in; #rsaraswat@nio.org)
ψ Now at: Department of Earth Sciences, Indian Institute of Technology Roorkee, India

Abstract

Modern observations and model simulations suggest a strong influence of tropical processes on high-latitude climate. The evidence of similar tropics-high latitude climate link during glacial termination is, however, elusive. Here we show a strong influence of tropical processes in terminating the last glacial period based on multi-decadal seawater temperature, upwelling intensity and runoff records from the tropical Indian Ocean. We report a well-defined warming (1.4°C) starting at ~20 kyr BP coeval with abrupt increase in upwelling intensity and local CO₂ outgassing, long before the beginning of increase in global atmospheric CO₂ at 18.2 kyr BP. We suggest that the tropical Indian Ocean warming prior to the increase in global atmospheric CO₂ was modulated by intense regional hydrographic changes caused by local summer insolation. The warming prior to Termination I (~18-11 kyr BP), at our site was synchronous with a small but evident strengthening of the Atlantic Meridional Overturning Circulation (AMOC). We conclude that the early warming in the tropical northern Indian Ocean led to stronger AMOC and the subsequent melting of the northern high latitude sea ice, which ultimately triggered the Heinrich Stadial during the last glacial termination.

Keywords: Termination I, Tropical Indian Ocean, Mg/Ca-SST, global atmospheric CO₂, AMOC

1. Introduction

Prior to the industrialization, earth's climate fluctuated between long gradual glacial periods followed by rapid deglaciations leading to brief interglacial. Understanding the precise mechanism of the relatively abrupt switch from the long glacial to the brief interglacial, called termination, is one of the biggest challenges in the paleoclimate research (Archer et al., 2000; Sigman and Boyle, 2000; Sigman et al., 2010; Cheng et al., 2016). The astronomical forcing induced summer insolation changes in the northern high latitudes (Milankovitch cycles) have been suggested as the major driver of the glacial-interglacial cycles (Hays et al., 1976; Muller and MacDonald, 1997). Incoming solar radiation primarily controls the Milankovitch cycles, that triggers climate feedback mechanisms. Long term data suggest that the Northern Hemisphere summer insolation changes initiated the last four terminations (Ramyo, 1997), with the last one starting at ~18 kyr BP and known as Termination I. However, temperature increase during Termination I was nonlinear, including several cold stadial (Heinrich Stadial 1, HS1=~15-18 kyr BP; and Younger/Older Dryas, YD=11.6-12.9 kyr BP) and warm interstadial (Bølling-Allerød, B-A=12.9-14.7 kyr BP) intervals, despite of a linear increase in solar insolation. These so-called stadials and interstadials were tightly coupled with Atlantic Meridional Overturning Circulation (AMOC) weakening and strengthening, respectively (McManus et al., 2004). AMOC variability was also associated with atmospheric CO₂ outgassing (Anderson et al., 2009). AMOC weakening during HS1 and YD caused a southward movement of the Northern Hemisphere westerlies and intense upwelling in the Southern Ocean (Menviel et al., 2018), whereas strengthened AMOC during B-A was coupled with warming in the Northern Hemisphere, a northward movement of Intertropical Convergence Zone (ITCZ) and intense upwelling in the Northern Hemisphere (Gray et al., 2018) including the Arabian Sea (Palmer et al., 2010; Naik et al., 2015). It has been suggested that pre-warming along with the release of heat from warm waters in the deep North Atlantic Ocean triggered the Bølling–Allerød warming and reinvigoration of the AMOC (Thiagarajan et al., 2014).

Tropical regions receive more solar energy and have a greater amount of heating per unit of area. Thus, the tropical ocean strongly modulates the total heat budget of the Earth (Hastenrath, 1980; Rao and Sivakumar, 2000; Alory and Meyers, 2009). Recent findings suggest that the tropical Indian Ocean has been storing more than 70% of the global ocean heat during the last decade (Lee et al., 2015) and concurrent strengthening the ocean circulation/AMOC (Hu and Fedorov, 2019). A strong influence of the tropical warming by transferring heat to the high northern latitudes via an atmospheric bridge has also been suggested (Rodgers et al., 2003). Modern observations suggest a strong influence of the tropical processes in modulating high latitude climate variability with implications for the past climatic variability (Cane, 1998; Clement et al., 2001; Clem et al., 2018). Amongst the tropics, warmer tropical Indian Ocean enhances precipitation and hence latent heat release, inducing a global-scale

Gill-type atmospheric response with pronounced stationary Kelvin waves that strengthen the Walker cell over the Atlantic Ocean and thus, cools the eastern and central equatorial Atlantic sea surface temperature (SST) (Hu and Fedorov, 2019). A cooler SST leads to reduced rainfall and a saltier tropical South Atlantic, which advects northward and contributes to denser surface waters in the subpolar North Atlantic and a strengthened AMOC (Hu and Fedorov, 2019). These point towards a strong influence of the Indian Ocean on post-industrialization climate.

Whether tropical Indian Ocean warming contributed to the past global warming/glacial termination in the same manner, remains elusive. Both the model and proxy data suggest an evident interval (~19-20 kyr BP) of AMOC strengthening (Shakun et al., 2012; Ehlert and Levermann, 2014) prior to its collapse during the HS1. The sea ice also started to retreat at ~20 kyr BP in the Northern Hemisphere (Denton et al., 2010), concurrent to the AMOC strengthening. So far, the cause of the initial strengthening of AMOC and the subsequent glacial termination is debated. Although the northern tropical Indian Ocean causes AMOC strengthening during the modern time, its role on the initial strengthening of AMOC prior to the last termination is not explored yet owing to the lack of high resolution regional SST (Anand et al., 2008; Govil and Naidu, 2010; Saraswat et al., 2013) records of Termination I.

2. Materials and Method

The gravity core SSD004 GC03 was recovered from 1540 m water depth onboard *RV Sindhu Sadhana*, from the tropical Indian Ocean (7.2254°N, 77.9458°E) (Figure 1). The core was sub-sampled at 1 cm interval. The sub-samples were processed by following standard procedure and were wet-sieved at 63 µm. The coarse fraction (>63 µm) was dry-sieved at 250 µm and 350 µm. For the stable isotopic and trace elements analyses, 35-40 shells of surface-dwelling planktic foraminifera *Globigerinoides ruber* (sensu stricto) were picked from 250-350 µm size fraction. The relative abundance (%) of *Globigerina bullioides* has been calculated from >150 µm size fraction. The relative abundance of planktic foraminifera *Globigerina bulloides* is used as a proxy for changes in wind-induced upwelling of sub-surface waters (Naidu and Malmgren, 1996). The freeze-dried and finely powdered sediments were used for the total and inorganic carbon analysis. The total carbon was analyzed by using the Flash 2000 series CN Elemental Analyzer and the inorganic carbon was measured by using coulometer (model CM 5015 CO₂). The organic carbon percentage in the sediments was estimated by subtracting the inorganic carbon from the total carbon.

2.1 Isotopic and Trace elements analysis

Globigerinoides ruber (s.s.) were picked (5-10 shells) for the stable isotopic ($\delta^{18}\text{O}$) analysis. The measurements were done at MARUM, University of Bremen, Germany, using Thermo Fisher Scientific 253 plus gas isotope ratio mass spectrometer with Kiel IV automated carbonate preparation device. The standard deviation of in-house standard (Solnhofen limestone) over measurement period was 0.05‰ for $\delta^{18}\text{O}$. For trace element analysis, *G. ruber* tests were cleaned by following the method developed by Barker et al. (2003), with a few modified steps. 25-30 shells were gently crushed under clean glass slide and transferred to centrifuge tubes. The crushed specimens were washed five times with ultra-high-quality water (UHQ) with frequent ultrasonic bath after each wash and then rinsed with ethanol two times to remove clay mineral contamination. After that, the samples were treated with hydrogen peroxide (H_2O_2) buffered with 0.1 M NaOH in a boiling water bath for 10 minutes (every 2.5 minutes, ultrasonic cleaning for 30 seconds was applied) to oxidize organic matter. A short (30 seconds) dilute acid leaching process was also applied by using 0.001 M HNO_3 to remove any adsorbed (Fe-Mn overgrowth/coating) contamination from test fragments. Prior to the measurements, the samples were dissolved in 500 μl of 0.075 M HNO_3 and centrifuged for 10 minutes at 6000 rotations per minute. The samples were then transferred into test tubes and diluted. The trace elements (Mg, Ba, Sr, Mn, Al and Fe) were measured along with major element calcium (Ca). The elements were measured by using Agilent Technologies 700 Series Inductively Coupled Plasma-Optical Emission Spectrometer equipped with an autosampler (ASX-520), at MARUM, University of Bremen, Germany. Mg/Ca values are reported as mmol/mol and Ba/Ca as $\mu\text{mol/mol}$. The instrumental precision was determined by using an in-house (Mg/Ca=2.92 mmol/mol) standard run after every fifth sample and ECRM 752-1 (Mg/Ca=3.75 mmol/mol) standard, run after every fifty samples. The standard deviation of in-house and ECRM 752-1 standard was ± 0.04 (0.14% rsd) (rsd= relative standard deviation) and ± 0.03 (0.38% rsd), respectively. The average Fe/Ca (≤ 0.1 mmol/mol), Al/Ca (0.005 mmol/mol) and Mn/Ca (≤ 0.04 mmol/mol) were below the threshold for contamination (1.0 mmol/mol; Barker et al., 2003). Additionally, no correlation was found between Mg/Ca and Fe/Ca ($r^2=0.002$), Al/Ca ($r^2=0.006$) and Mn/Ca ($r^2=0.061$) confirming the efficiency of the cleaning procedure and the absence of contamination. The replicate measurements were performed on 20 samples, and have an average standard deviation of 0.12 mmol/mol. For the SST error estimate, the equation provided by Mohtadi et al. (2014) was used assuming no covariance among the errors. The error in SST, calculated according to this equation was $\sim 0.9^\circ\text{C}$.

The SST was estimated from the Mg/Ca ratio of the surface-dwelling planktic foraminifera *Globigerinoides ruber* (s. s.) by using the equation given by Anand et al. (2003). This equation gives

the closest temperature value in the core top as compared to the modern SST (27.4°C) at the core site. The $\delta^{18}\text{O}$ of seawater was calculated by using Mg/Ca derived SST and $\delta^{18}\text{O}_{ruber}$ by using the Bemis et al. (1998) equation. The $\delta^{18}\text{O}_{ruber}$ was corrected for sea-level changes ($\delta^{18}\text{O}_{sw-ivc}$), reconstructed by Waelbroeck et al. (2002) and converted to Vienna Standard Mean Ocean Water (SMOW) by adding 0.27‰ to $\delta^{18}\text{O}_{sw-ivc}$. The error associated with the ice volume corrected $\delta^{18}\text{O}_{sw}$ was 0.3‰. The $\delta^{18}\text{O}_{sw-ivc}$ error was calculated according to Mohtadi et al. (2014).

The field and laboratory culturing studies suggests that planktic foraminiferal Ba/Ca can be used as a proxy for riverine influx (Lea and Spero, 1994; Waldeab et al., 2007; Saraswat et al., 2013). The Ganga-Brahmaputra runoff strongly modulates the surface seawater Ba in the entire Bay of Bengal, including the southern part, close to the core location. The surface water (<5 m) Ba concentration is higher than the deep water (>5 to ~150 m) (Singh et al., 2013). Foraminiferal Ba/Ca ratio is, however, also influenced by upwelling (Saraswat et al., 2013) and sulfate reduction in the eastern Arabian Sea during Holocene (Agnihotri et al., 2003). The upwelling induced higher productivity dissolves the barite (BaSO_4) in the sediments and releases Ba into pore waters, ultimately causing increased Ba precipitation onto the foraminiferal shells. The average error associated with the Ba/Ca, based on replicate measurements ($n = 20$), was 0.24 $\mu\text{mol/mol}$.

2.2 Chronology

The chronology of SSD004 GC03 core was established by using 13 Accelerator Mass Spectrometer (AMS) radiocarbon (^{14}C) dates on surface mixed layer planktic foraminifera (*Globigerinoides ruber* + *Trilobatus sacculifer*) (Table 1). In addition to this, 2 AMS dates were done on benthic foraminifera (*Cibicidoides wuellerstorfi* + *Cibicidoides pachyderma*). The radiocarbon dates were measured at the Inter-University Accelerator Center, Delhi, India. The age-depth model was prepared by Bacon software (Blaauw et al., 2011) by using Marine13 calibration curve (Reimer et al., 2013). A local reservoir age correction (ΔR) of 36 ± 8 yr (Dutta et al., 2001) was applied to account for the difference in radiocarbon age of the seawater and the atmosphere, to calibrate the radiocarbon ages.

3. Results

The studied section covers the entire last glacial-interglacial transition (8-24 kyr BP). The sedimentation rate varied from 4.53 cm/kyr (between 16.0-17.5 kyr BP) to 31.19 cm/kyr (between 9.8-11.2 kyr BP), with an average of 15.31 cm/kyr during the studied section. The age difference between surface and bottom water was 445 yr at 19.7 kyr BP and increased to 1348 yr during Heinrich Stadial 1.

The Mg/Ca derived glacial-interglacial SST difference was $\sim 4^{\circ}\text{C}$. During the LGM (19-23 kyr BP), average SST was $25.3 \pm 0.6^{\circ}\text{C}$. Deglacial warming started at 18.2 kyr BP and progressed in two-steps. First rapid warming episode was between 18.2-17.2 kyr BP when SST warmed by 2.5°C within this short time span (Fig. 2). A short warming phase between 19.7-18.2 kyr BP, however, preceded the subsequent rapid deglacial warming. The second warming phase was during the Younger Dryas. In the remaining part of HS1 as well as Bølling-Allerød interstadial (12.7 - 14.7 kyr BP), SST remained stable and varied only within the 1σ error ($26.4 - 27.6 \pm 0.3^{\circ}\text{C}$). However, during the Younger Dryas (11.7- 12.9 kyr BP), SST was higher ($1.2 \pm 0.3^{\circ}\text{C}$) than the preindustrial temperature and $\sim 1.8^{\circ}\text{C}$ warmer than the preceding interval (Fig. 2).

A large variation in $\delta^{18}\text{O}$ (-2.66 to -0.23‰) was observed during the studied interval. The most enriched $\delta^{18}\text{O}$ was during the LGM and decreased continuously afterwards, except during YD when values slightly increased (Fig. 2). During the Termination 1, ice volume corrected $\delta^{18}\text{O}_{\text{sw}}$ varied between -0.01 to 1.21‰ . The highest $\delta^{18}\text{O}_{\text{sw-ivc}}$ was at 16.2 kyr BP. During B-A, $\delta^{18}\text{O}_{\text{sw-ivc}}$ showed a steady increase with an average of 1.97‰ which is $\sim 2\text{‰}$ higher than LGM (0.04‰) (Fig. 2). During the Termination 1, Ba/Ca varied between 1.3 to $2.7 \mu\text{mol/mol}$ (Fig. 2). A large decrease in Ba/Ca was observed between 19.5 kyr BP and 16.4 kyr BP. Subsequently, Ba/Ca increased until 12.5 kyr BP, with some fluctuations in-between. The relative abundance of *G. bulloides* varied from a maximum of 28.6% at 21.6 kyr BP to the minimum of 2.6% during the Termination 1 (16.2 kyr BP). A distinct phase of high *G. bulloides* relative abundance was observed between 19.7-17.5 kyr. The relative abundance was high during the LGM. The lowest concentration of organic carbon ($\%C_{\text{org}}$) was at 16.4 kyr BP (1.4%). Before that, a distinct phase of increased $\%C_{\text{org}}$ was observed between 19.7 to 18.2 kyr BP. After HS1, a continuous increase in $\%C_{\text{org}}$ was observed in our record except during YD, when $\%C_{\text{org}}$ concentration decreased significantly.

Discussion

3.1 Comparison with regional records

Our Mg/Ca SST record shows $\sim 4^{\circ}\text{C}$ glacial-interglacial change (Fig. 3). The incorporation of Mg in calcareous planktic foraminifera shells is temperature dependent and thus the Mg/Ca ratio of planktic foraminifera is frequently used to quantify the past SST (Nürnberg et al., 1996; Lea et al., 2000; Mohtadi et al., 2014; Saraswat et al., 2019). Although the ambient seawater pH and salinity also influence the Mg incorporation in the calcareous shells, the temperature exerts the dominant control (Gray and Evans, 2019). The deglacial warming in the northern Indian Ocean responds to summer insolation changes and atmospheric CO_2 rise (Saraswat et al., 2013).

During HS1, our plateau-like warm SST resembles those from the eastern (Mohtadi et al., 2014) and central equatorial Indian Ocean (Anand et al., 2008; Saraswat et al., 2013) but differs from a cooler western Indian Ocean (Tierney et al., 2016) (Figure 3). During YD, $\sim 1.2 \pm 0.3^\circ\text{C}$ warming in SSD004 GC03 is within the same range ($\sim 1^\circ\text{C}$) as in the Bay of Bengal (Panmei et al., 2017), whereas no significant warming is observed in the southeastern Arabian Sea (Saraswat et al., 2013). The beginning of deglacial warming between 18-19 kyr BP, is synchronous in almost all the records from the northern Indian Ocean (Figure 3). The initial rapid warming phase in our record is also observed in the Andaman Sea (Liu et al., 2021).

$\delta^{18}\text{O}_{\text{sw-ivc}}$ progressively increased towards the later part of LGM until 16.2 kyr, suggesting a continuous weakening of the monsoon (Fig. 4). This finding is in agreement with previous results (Saraswat et al., 2013; Mohtadi et al., 2014), including the low-resolution records (Govil and Naidu, 2011), suggesting a weaker southwest monsoon and a reduced inflow of Bay of Bengal water in this region during the later phase of LGM (Mahesh and Banakar, 2014). Likewise, a decrease in Ba/Ca values in the Andaman Sea has also been interpreted to reflect a weaker ISM rainfall, i.e. a weaker southwest monsoon, and saltier conditions in the Bay of Bengal during a part of the LGM (Gebregiorgis et al., 2016). The decrease in Ba/Ca ($\sim 1.0 \pm 0.3\%$) during the corresponding later part of the LGM, also confirms reduced riverine runoff in the vicinity of core site. The findings clearly suggest that the changes in Ba/Ca effectively trace variations in riverine runoff (Saraswat et al., 2013).

During HS1, the weakest monsoon period is evident from the highest $\delta^{18}\text{O}_{\text{sw-ivc}}$ at the core site in line with results from other studies (Saraswat et al., 2013; Mohtadi et al., 2014; Tierney et al., 2016). Combined with the lowest Ba/Ca during this interval ($1.3 \pm 0.4\%$), our results suggest that during the early HS1, both the southwest and the northeast monsoon wind and rainfall were weak. The subsequent decrease in $\delta^{18}\text{O}_{\text{sw-ivc}}$ and increase in Ba/Ca suggest a rebounding monsoon towards the late HS1. An intensification of monsoon towards the end of HS1 and beginning of B-A was proposed from sediment cores in the western Arabian Sea (Tierney et al., 2016), the eastern Arabian Sea (Kessarkar et al., 2013), and the Andaman Sea (Gebregiorgis et al., 2016).

Depleted $\delta^{18}\text{O}_{\text{sw-ivc}}$ in our record during B-A suggest a major intensification of the southwest monsoon in line with records from both the eastern Arabian Sea and Bay of Bengal (Govil and Naidu, 2011; Kessarkar et al., 2013). Within B-A, an episode of enriched $\delta^{18}\text{O}_{\text{sw-ivc}}$ was found around 13.5 kyr BP, which shows similarity with the western Arabian Sea (ODP 723 A; Gupta et al., 2013) suggesting a weak southwest monsoon during Allerød. During YD, $\delta^{18}\text{O}_{\text{sw-ivc}}$ increased suggesting a weaker monsoon period, as reported previously from the northern (Anand et al., 2008) and eastern Indian Ocean (Mohtadi et al., 2014). Interestingly, the variations in monsoon intensity, as inferred from the

marine core SSD004 GC03, very well match with the terrestrial cave speleothem oxygen isotope (Dutt et al., 2015) and lake leaf wax hydrogen isotope based monsoon records (Zhao et al., 2021) (Fig. 4).

3.2 Global Implications

In light of the strong present-day influence of the Indian Ocean warming on the AMOC, we explored the nature of warming during the Termination I in the northern tropical Indian Ocean and its potential effect on the AMOC. At our site, Termination I at 18.2 kyr BP is characterized by a rapid warming of 2.5°C within 600-700 years (Fig. 2). The timing of this warming at our site in the tropical Indian Ocean is synchronous with the initial increase in the atmospheric CO₂ recorded in the EPICA Dome C ice core (Parrenin et al., 2013) (Fig. 3). During the globally synchronous, initial rapid warming phase of the Termination 1 that coincides with the complete shutdown of AMOC (McManus et al., 2004; Shakun et al., 2012), $\delta^{18}\text{O}_{\text{sw-ivc}}$ at our site remained high, while both the Ba/Ca ratio and the relative abundance of *G. bulloides* (%) remained constant at a relatively low level (Fig. 2). During the B-A interstadial, SST was stable and varied only within the 1 σ error (26.4 - 27.6 \pm 0.3°C). During the YD stadial, SST warmed by 1.2 \pm 0.3°C, while *G. bulloides* abundance increased from 8 to 19%, and $\delta^{18}\text{O}_{\text{sw-ivc}}$ increased by 0.86‰ (Fig. 3). Overall, our results indicate that during the period of northern high latitudinal stadials/AMOC weakening, SST in the tropical Indian Ocean increased rather abruptly by 1-2°C. The findings are in line with the previous reports that also suggest a net warming of the tropical Indian Ocean during stadials (Mohtadi et al., 2014; Panmei et al., 2017).

A very intriguing feature of our SST record is a distinct warming phase prior to the Termination I, beginning at 19.7 kyr BP (1 σ = 19.5-20.2 kyr BP). A comparison of our record with other regional data clearly indicates a similar event in several other locations, suggesting its basin-wide nature (Fig. 3) (Govil and Naidu, 2011; Mohtadi et al., 2014; Kumar et al., 2021). The onset of warming at our site corresponds well with the increase in local (7°N) July insolation between 19-20 kyr (Laskar et al., 2004) (Fig. 3). The evidently synchronous change in SST and insolation rise reconciles earlier ambiguity in the lag of SST rise as compared to the increase in summer insolation, indicated by several records from this region with a comparatively lower temporal resolution (Fig. 3; Anand et al., 2008; Govil and Naidu, 2010; Saraswat et al., 2013; Gibbons et al., 2014; Mohtadi et al., 2014). In this warming phase (between 19.7-18.2 kyr BP), SST warmed by as much as 1.4°C, as compared to the background value (Fig. 3). This warming phase was concurrent with last ice recession in the Northern Hemisphere at ~20 kyr BP (Denton et al., 2010) but precedes the global deglacial warming by >1-2 kyr and is different from the majority of the records from the northern Indian Ocean, where only a warming step at ~17 kyr BP is reported (Fig. 3; Anand et al., 2008; Govil and Naidu, 2010). The difference might be either due to the uncertainties in the age models, the relatively coarse temporal

resolution of the previous records, or the use of different *G. ruber* morphotypes (sensu stricto/sensu lato). The depth habitat of *G. ruber* sensu stricto and sensu lato is different. *Globigerinoides ruber* sensu lato morphotype lives at deeper water depths as compared to *G. ruber* sensu stricto morphotype, and thus precipitates its shells in slightly colder water, resulting in difference in Mg/Ca based temperature estimates (Steinke et al., 2005). Thus the extent of SST rise during the early Termination might differ when using different *G. ruber* morphotypes (Mohtadi et al., 2010). This warming phase in the tropical Indian Ocean leads the AMOC slowdown starting at ~19.0 kyr BP (McManus et al., 2004; Shakun et al., 2012) by ~1.0 kyr (Fig. 5). The lead of this warming phase in the tropical Indian Ocean over the beginning of the atmospheric CO₂ rise, ice-volume changes as well as the AMOC slowdown, clearly points towards other processes modulating the northern tropical Indian Ocean SST.

Interestingly, this initial warming phase between 19.7-18.2 kyr BP was accompanied by an increase in upwelling intensity, as evident from an abrupt increase in the relative abundance of *G. bulloides* (from $8.0 \pm 1\%$ to $17.5 \pm 1\%$). The relative abundance of *G. bulloides* is a robust indicator of wind-induced upwelling in the Arabian Sea (Naidu et al., 1995; Singh et al., 2011). *Globigerina bulloides* prefers regions with high productivity and relatively cold waters (Darling et al., 2017). The monsoon wind induced upwelling brings the nutrient rich relatively cold sub-surface water to the surface. The upwelling of nutrient rich cold water facilitates productivity at the surface. Thus, the relative abundance of *G. bulloides* is used as a proxy to infer upwelling strength and the monsoon intensity in the past (Naidu et al., 1995; Singh et al., 2011). The strong upwelling prior to Termination I is further supported by a lower difference in ventilation age, as compared to non-upwelling intervals. We measured the radiocarbon (¹⁴C) age of surface mixed layer dwelling planktic foraminifera (*G. ruber* + *T. sacculifer*) as well as benthic foraminifera (*C. wuellerstorfi* + *C. pachyderma*). The radiocarbon age difference between the bottom waters inferred from benthic foraminifera data, and surface waters inferred from surface-dwelling planktic foraminifera data, was minimum (445 yr) at 19.7 kyr BP (Table 1). The difference increased to 1348 yr during HS1 when upwelling was the weakest. This phase of increased surface productivity and subsequent organic matter flux to the bottom, is also evident from the increase in %C_{org}. However, it should be noted here that the %C_{org} in sediments depends on several factors, including the grain-size, sedimentation rate and dissolved oxygen at the sediment-water interface. The regional nature of this upwelling induced increased productivity and its effect of global carbon-dioxide concentration is also evident from the nitrogen isotopic records from the Arabian Sea (Altabet et al., 2002; Kao et al., 2015).

The intense upwelling at the peak of glaciation is intriguing and coincides with a rise in local summer insolation (Fig. 5). A rise in the local insolation alone is, however, a too weak forcing to cause

termination (Denton et al., 2010) and needs amplifying mechanisms, besides that this does not explain the local upwelling increase. One mechanism that might explain this anomalous upwelling in the deep glacial is the fact that the Northern Hemisphere was relatively cooler as compared to the Southern Hemisphere (more land mass), resulting in a stronger inter-hemispheric temperature gradient (Fig. 6). This energy imbalance had to be compensated by the ocean and/or by the atmosphere, and excited the cross-equatorial ocean currents and winds to transport heat from the warmer Southern Hemisphere to the cooler Northern Hemisphere (Bordoni and Schneider, 2008) (Fig. 6). Those winds are an integral part of the upwelling in the northern tropical Indian Ocean. The resulting increase in summer upwelling in the Arabian Sea and the release of CO₂ might have been the amplifying feedbacks needed for the glacial termination (Fig. 6), in accordance with previous studies that identify the Arabian Sea as a source of atmospheric CO₂ during the Termination I (Palmer et al., 2010; Naik et al., 2015). Interestingly, Cuffey et al. (2016) also reported early Antarctic warming and attributed it to insolation and greenhouse forcing with possible contribution from the tropical processes.

Generally, upwelling strongly decreases the SST as it brings cooler and nutrient-rich water to the surface (de Boyer et al., 2007). The warming recorded at our site in spite of the increase in upwelling indicates that the extent of warming was such that it exceeded the cooling of the surface waters by upwelling of subsurface waters during boreal summer. The upwelling is mainly during the summer season, in response to the strong winds (Chatterjee et al., 2019). The summer monsoon wind induced upwelling brings cold, nutrient rich sub-surface water to the surface (Bakun, 1990). Therefore, upwelling causes seasonal cooling of surface seawater temperature (Chatterjee et al., 2019) and increases productivity due to nutrient entrainment in the surface mixed layer (Sreeush et al., 2018). During the rest of the year, insolation affects the seawater temperature. The insolation began to increase by ~20 kyr BP. The pre-deglacial warming phase is attributed to the increase in insolation, as the tropical ocean rapidly responds to the insolation. The increased insolation caused net warming despite of the seasonal upwelling induced cooling. The warming induced intense upwelling is observed in several modern field and modelling studies (Bakun, 1990; Xiu et al., Praveen et al., 2016; 2018). The upwelling also significantly increases the CO₂ flux thus affecting the atmospheric CO₂ concentration (Sreeush et al., 2018). Additionally, the increased influx of relatively fresher water, as evident from the episodic increase in Ba/Ca coinciding with the intense upwelling interval, might have further facilitated the early warming (Saraswat et al., 2013). The increased runoff is further supported by depleted $\delta^{18}\text{O}_{\text{sw-ivc}}$ during the later part of the intense upwelling interval. Previously, a similar increased productivity and terrestrial input in the southeastern Arabian Sea between 17-25 kyr BP, was also inferred from the higher %C_{org}, C/N ratio, $\delta^{13}\text{C}_{\text{org}}$, carbon preference index (CPI) of n-alkanes and

n-alkanols in a gravity core (CC2-GCEq2, 2°29' N latitude and 78°E longitude) (Punyu et al., 2014). The terrestrial records from the summer monsoon influenced regions of India as well as China, also have a brief intense monsoon interval prior to HS1 (Dutt et al., 2015; Zhao et al., 2021).

We suggest that the initial phase of tropical warming strengthened the AMOC, by weakening the monsoon over the tropical Atlantic and strengthening the westerly winds in the subpolar North Atlantic, causing enhanced transfer of heat to the high northern latitudes (Hu and Fedorov, 2019). The increased transport of warmer waters to the high northern latitudes then melted the ice-sheets, causing the subsequent complete collapse of the AMOC. It was suggested earlier that the insolation-induced melting played an important role in suppressing the AMOC during HS1 (He et al., 2013) and the resulting melt-water flux likely served as the initial trigger for AMOC weakening (McManus et al., 2004; Carlson and Clark, 2012). The warming observed during the same interval in the NGRIP ice core record supports the hypothesis of a warming northern high latitudinal region in response to early tropical warming. The modelling results also show that the early warming of tropical SST in response to increasing insolation towards the end of glacial intervals caused a large increase in northern high latitudinal summer temperatures (Rodgers et al., 2003).

Conclusion

We reconstruct the sub-centennial seawater temperature, upwelling intensity, runoff and monsoon record of the last Termination from the northern Indian Ocean. The deglacial warming in this core, was synchronous with other high-resolution tropical Indian Ocean warming records. Interestingly, a distinct warming phase, just prior to the deglaciation, is also observed in this tropical Indian Ocean record and was modulated by intense regional hydrographic changes caused by local summer insolation. We propose that this pre-deglaciation tropical warming phase strengthened the AMOC, which led to increased heat transport towards the northern high latitude, a critical precondition for the melting of the high latitude ice sheet and the subsequent weakening and complete collapse of the AMOC during HS1, and global atmospheric CO₂ rise. Our proxy data suggest that the tropical Indian Ocean upwelling also contributed to the rise in atmospheric CO₂ during the deglaciation. However, further studies are required to quantify the extent of the tropical Indian Ocean contribution to the atmospheric CO₂.

Acknowledgements

Authors are thankful to the Council of Scientific and Industrial Research, Government of India for financial support. DPS acknowledges the fellowship provided by DAAD, Germany. Authors thank the support staff at MARUM, Germany for the help in elemental and isotopic analysis. Authors also

acknowledge the Inter University Accelerator Center for extending the graphitization laboratory and Accelerator Mass Spectrometer measurement facility for ^{14}C established under the Ministry of Earth Science (MoES) funded projects (MoES/16/07/11(i)-RDEAS). Data archiving is underway, the same has been submitted to PANGAEA - Data Publisher for Earth & Environmental Science (Ticket No: PDI-28360). Please find dataset as supporting files for the review process.

Author contributions

RS conceived the research idea and further developed it with DPS. DPS processed the samples, picked foraminifera, and conducted foraminifera cleaning and trace element analysis under the guidance of MM at Marum, Bremen. PK performed radiocarbon dating on planktic as well benthic foraminifera. RS, DPS and MM discussed data interpretation and wrote the manuscript. All authors contributed to the final text.

References:

- Agnihotri, R., Sarin, M.M., Somayajulu, B.L.K., Jull, A.J.T. & Burr, G.S. Late-Quaternary biogenic productivity and organic carbon deposition in the eastern Arabian Sea. *Palaeogeogr. Palaeoclimatol. Palaeoecol.* 197, 43-60 (2003).
- Alory, G. & Meyers, G. Warming of the upper equatorial Indian Ocean and changes in the heat budget (1960–99). *J. Clim.* 22, 93-113 (2009).
- Anand, P. et al. Coupled sea surface temperature seawater $\delta^{18}\text{O}$ reconstructions in the Arabian Sea at the millennial scale for the last 35 ka. *Paleoceanography* 23 (2008).
- Anand, P., Elderfield, H. & Conte, M.H. Calibration of Mg/Ca thermometry in planktonic foraminifera from a sediment trap time series. *Paleoceanography* 18 (2003).
- Anderson, R. F. et al. Wind-driven upwelling in the Southern Ocean and the deglacial rise in atmospheric CO_2 . *Science* 323, 1443-1448 (2009).
- Archer, D., Winguth, A., Lea, D. & Mahowald, N. What caused the glacial/interglacial atmospheric pCO_2 cycles? *Rev. Geophys.* 38, 159–189 (2000).
- Bakun, A. Global Climate Change and Intensification of Coastal Ocean Upwelling. *Science*, 247, 198-201 (1990).
- Barker, S., Greaves, M. & Elderfield, H. A study of cleaning procedures used for foraminiferal Mg/Ca paleothermometry. *Geochem. Geophys. Geosys.* 4, 1-20 (2003).
- Bemis, B. E., Spero, H. J., Bijma, J. & Lea, D. W. Reevaluation of the oxygen isotopic composition of planktonic foraminifera: Experimental results and revised paleotemperature equations. *Paleoceanography* 13, 150-160 (1998).
- Blaauw, M. & Christen, J.A., Flexible paleoclimate age-depth models using an autoregressive gamma process. *Bayesian Anal.* 6, 457-474 (2011)

- Bordoni, S. & Schneider, T. Monsoons as eddy-mediated regime transitions of the tropical overturning circulation. *Nat. Geosci.* 1, 515-519 (2008).
- Cane, M.A. A role for the tropical Pacific. *Science* 282, 59-61 (1998).
- Carlson, A. E. & Clark, P.U. Ice sheet sources of sea level rise and freshwater discharge during the last deglaciation. *Rev. Geophys.* 50, RG4007 (2012).
- Chatterjee, A., B.P. Kumar, S. Prakash & P. Singh. Annihilation of the Somali upwelling system during summer monsoon. *Sci. Rep.* 9, 7598 (2019).
- Cheng, H., Edwards, R., Sinha, A., Spötl, C., Yi, L., Chen, S., Kelly, M., Kathayat, G., Wang, X., Li, X., Kong, X., Wang, Y., Ning, Y., Zhang, H. The Asian monsoon over the past 640,000 years and ice age terminations. *Nature* 534, 640–646 (2016).
- Clem, K. R., Renwick, J. A. & McGregor, J. Autumn cooling of western East Antarctica linked to the tropical Pacific. *J. Geophys. Res. Atmos.* 123, 89-107 (2018).
- Clement, A.C., Cane, M.A. & Seager, R. An orbitally driven tropical source for abrupt climate change. *J. Clim.* 14, 2369-2375 (2001).
- Darling, K.F., C.M. Wade, M. Siccha, G. Trommer, H. Schulz, S. Abdolalipour, A. Kurasawa. Genetic diversity and ecology of the planktonic foraminifers *Globigerina bulloides*, *Turborotalita quinqueloba* and *Neogloboquadrina pachyderma* off the Oman margin during the late SW Monsoon. *Mar. Micropaleontol.* 137, 64-77 (2017).
- de Boyer Montégut, J. et al. Simulated seasonal and interannual variability of mixed layer heat budget in the northern Indian Ocean. *J. Climate* 20, 3249-3268 (2007).
- Denton, G. H. et al. The last glacial termination. *Science* 328, 1652-1656 (2010).
- Dutt, S., A.K. Gupta, S. C. Clemens, H. Cheng, R. K. Singh, G. Kathayat, R. L. Edwards 2015. Abrupt changes in Indian summer monsoon strength during 33,800 to 5500 years B.P. *Geophys. Res. Lett.*, 42, 5526–5532.
- Dutta, K., Bhushan, R. & Somayajulu, B.L.K. ΔR correction values for the northern Indian Ocean. *Radiocarbon* 43, 483–488 (2001).
- Ehlert, D. & Levermann, A. Mechanism for potential strengthening of Atlantic overturning prior to collapse. *Earth Syst. Dyn.* 5, 383-397 (2014).
- Govil, P. & Naidu, P.D. Evaporation-precipitation changes in the eastern Arabian Sea for the last 68 ka: Implications on monsoon variability. *Paleoceanography* 25, 1-11 (2010).
- Govil, P., Naidu, P.D. 2011. Variations of Indian monsoon precipitation during the last 32 kyr reflected in the surface hydrography of the Western Bay of Bengal. *Quaternary Science Reviews* 30, 3871-3879.
- Gray, W. R. et al. Deglacial upwelling, productivity and CO₂ outgassing in the North Pacific Ocean. *Nat. Geosci.* 11, 340-344 (2018).
- Hastenrath, S. Heat budget of tropical ocean and atmosphere. *J. Phys. Oceanogr.* 10, 159-170 (1980).

- Hays, J.D., Imbrie, J. & Shackleton, N.J. Variations in the Earth's orbit: Pacemaker of ice ages. *Science* 194, 1121–1132 (1976).
- He, F. et al. Northern Hemisphere forcing of Southern Hemisphere climate during the last deglaciation. *Nature* 494, 81–85 (2013).
- Hu, S. & A.V. Fedorov. Indian Ocean warming can strengthen the Atlantic meridional overturning circulation. *Nat. Clim. Change*. 9, 747–751 (2019).
- Kao, S.-J., Wang, B.-Y., Zheng, L.-W., Selvaraj, K., Hsu, S.-C., Sean Wan, X. H., Xu, M., Arthur Chen, C.-T. Spatiotemporal variations of nitrogen isotopic records in the Arabian Sea, *Biogeosciences*, 12, 1–14 (2015).
- Kumar, V., Tiwari, M., Prakash, P., Mohan, R., & Thamban, M. SST changes in the Indian sector of the Southern Ocean and their teleconnection with the Indian monsoon during the last glacial period. *Paleoceanogra. Paleoclimatol.* 36, e2020PA004139 (2021).
- Laskar, J. et al. A long term numerical solution for the insolation quantities of the Earth. *Astron. Astrophys.* 428, 261–285 (2004).
- Lea, D. W. & Spero, H. J. Assessing the reliability of paleochemical tracers: Barium uptake in the shells of planktonic foraminifera. *Paleoceanography* 9, 445–452 (1994).
- Lea, D.W., Pak, D.K., Spero, H.J., 2000. Climate impact of late quaternary equatorial Pacific sea surface temperature variations. *Science* 289, 1719–1724.
- Lee, S. K. et al. Pacific origin of the abrupt increase in Indian Ocean heat content during the warming hiatus. *Nat. Geosci.* 8, 445–449 (2015).
- Liu, S., Wenxing Ye, Peng Cao, Hui Zhang, Min-Te Chen, Xiaoyan Li, Jingrui Li, Hui-Juan Pan, Somkiat Khokiattiwong, Narumol Kornkanitnan, Xuefa Shi. Paleoclimatic responses in the tropical Indian Ocean to regional monsoon and global climate change over the last 42 kyr. *Mar. Geol.* 438, 106542 (2021).
- Naidu, P. D., & Malmgren, B. A. (1996). A high-resolution record of late Quaternary upwelling along the Oman Margin, Arabian Sea based on planktonic foraminifera. *Paleoceanography*, 11(1), 129–140.
- McManus, J. F., Francois, R., Gherardi, J. M., Keigwin, L. D. & Brown-Leger, S. Collapse and rapid resumption of Atlantic meridional circulation linked to deglacial climate changes. *Nature* 428, 834–837 (2004).
- Menviel, L. et al. Southern Hemisphere westerlies as a driver of the early deglacial atmospheric CO₂ rise. *Nat. Commun.* 9, 1–12 (2018).
- Mohtadi, M. et al. North Atlantic forcing of tropical Indian Ocean climate. *Nature* 509, 76–80 (2014).
- Mohtadi, M., Steinke, S., Lückge, A., Groeneveld, J. & Hathorne, E.C. Glacial to Holocene surface hydrography of the tropical eastern Indian Ocean. *Earth Planet. Sci. Lett.* 292, 89–97 (2010).
- Muller, R. A. & MacDonald, G. J. Glacial cycles and astronomical forcing. *Science* 277, 215–218 (1997).

- Naidu, P.D. & Malmgren, B.A. Do benthic foraminifera records represent a productivity index in oxygen minimum zones? An evaluation from Oman margin, Arabian Sea. *Mar. Micropaleontol.* 26, 49-55 (1995).
- Naik, S. S., Naidu, P. D., Foster, G. L. & Martínez-Botí, M. A. Tracing the strength of the southwest monsoon using boron isotopes in the eastern Arabian Sea. *Geophys. Res. Lett.* 42, 1450-1458 (2015).
- Nürnberg, D., J. Bijma, C. Hemleben. Assessing the reliability of magnesium in foraminiferal calcite as a proxy for water mass temperatures. *Geochim. Cosmochim. Acta*, 60, 803-814, (1996).
- Palmer, M. et al. Multi-proxy reconstruction of surface water pCO₂ in the northern Arabian Sea since 29 ka. *Earth Planet. Sci. Lett.* 295, 49-57 (2010).
- Panmei, C., Divakar Naidu, P., & Mohtadi, M. Bay of Bengal Exhibits Warming Trend During the Younger Dryas: Implications of AMOC. *Geochem. Geophys. Geosyst.* 18, 4317-4325 (2017).
- Parrenin, F. et al. Synchronous change of atmospheric CO₂ and Antarctic temperature during the last deglacial warming. *Science* 339, 1060-1063 (2013).
- Praveen, V., Ajayamohan, R. S., Valsala, V., Sandeep, S. Intensification of upwelling along Oman coast in a warming scenario. *Geophys. Res. Lett.* 43, (2016).
- Punyu, V. R., Banakar, V. K., and Garg, A. Equatorial Indian Ocean productivity during the last 33kyr and possible linkage to Westerly Jet variability. *Mar. Geol.* 348, 44–51 (2014).
- Rao, R. R. & Sivakumar, R. Seasonal variability of near-surface thermal structure and heat budget of the mixed layer of the tropical Indian Ocean from a new global ocean temperature climatology. *J. Geophys. Res.* 105, 995-1015 (2000).
- Raymo, M. E. The timing of major climate terminations. *Paleoceanography* 12, 577-585 (1997).
- Reimer, P.J. et al. IntCal13 and Marine13 radiocarbon age calibration curves 0-50,000 yr cal BP. *Radiocarbon* 55, 1869-1887 (2013).
- Rodgers, K. B., Lohmann, G., Lorenz, S., Schneider, R. & Henderson, G. M. A tropical mechanism for Northern Hemisphere deglaciation. *Geochem. Geophys. Geosyst.* 4, 1046 (2003).
- Saraswat, R., Lea, D.W., Nigam, R., Mackensen, A. & Naik, D.K. Deglaciation in the tropical Indian Ocean driven by interplay between the regional monsoon and global teleconnections. *Earth Planet. Sci. Lett.* 375, 166-175 (2013).
- Saraswat, R., D.P. Singh, D.W. Lea, A. Mackensen, D.K. Naik. Indonesian throughflow controlled the westward extent of the Indo-Pacific Warm Pool during glacial-interglacial intervals. *Global Planet. Change*, 183, 103031 (2019).
- Shakun, J. D. et al. Global warming preceded by increasing carbon dioxide concentrations during the last deglaciation. *Nature* 484, 49–54 (2012).
- Sigman, D.M. & Boyle, E.A. Glacial/interglacial variations in atmospheric carbon dioxide. *Nature* 407, 859–869 (2000).

- Sigman, D.M., Hain, M.P. & Haug, G.H. The polar ocean and glacial cycles in atmospheric CO₂ concentration. *Nature* 466, 47–55 (2010).
- Singh, A. D. et al. 2011. Productivity collapses in the Arabian Sea during glacial cold phases. *Paleoceanography* 26 (2011).
- Singh, S. P., Singh, S. K. & Bhushan, R. Internal cycling of dissolved barium in water column of the Bay of Bengal. *Mar. Chem.* 154, 12-23 (2013).
- Sreeush, M. G., V. Valsala, S. Pentakota, K. V. S. R. Prasad, R. Murtugudde. Biological production in the Indian Ocean upwelling zones –Part 1: refined estimation via the use of a variable compensation depth in ocean carbon models. *Biogeosciences* 15, 1895–1918, (2018).
- Steinke, S., Chiu, H. Y., Yu, P. S., Shen, C. C., Löwemark, L., Mii, H. S., & Chen, M. T. (2005). Mg/Ca ratios of two *Globigerinoides ruber* (white) morphotypes: Implications for reconstructing past tropical/subtropical surface water conditions. *Geochemistry, Geophysics, Geosystems*, 6(11).
- Takahashi, T. et al. Climatological mean and decadal change in surface ocean pCO₂, and net sea–air CO₂ flux over the global oceans. *Deep Sea Res. Part II Top. Stud. Oceanogr.* 56, 554-577 (2009).
- Thiagarajan, N. et al. Abrupt pre-Bølling–Allerød warming and circulation changes in the deep ocean. *Nature* 511, 75-78 (2014).
- Waelbroeck, C. et al. 2002. Sea-level and deep water temperature changes derived from benthic foraminifera isotopic records. *Quat. Sci. Rev.* 21, 295-305 (2002).
- Weldeab, S., Lea, D. W., Schneider, R. R., & Andersen, N. (2007). 155,000 years of West African monsoon and ocean thermal evolution. *Science* 316, 1303-1307.
- Zhao, C., Cheng, J., Wang, J., Yan, H., Leng, C., Zhang, C., et al. Paleoclimate significance of reconstructed rainfall isotope changes in Asian monsoon region. *Geophys. Res. Lett.* 48, e2021GL092460 (2021).

Legend to Figures

- Figure 1:** The location of gravity core SSD004 GC03, in the northern tropical Indian Ocean. The color shadings are summer (July, August and September) SST. The dashed contours are the modern annual $\Delta p\text{CO}_2$ (μatm) signifying that the northern tropical Indian Ocean is a net source of the atmospheric CO_2 (Takahashi et al., 2009). Red Arrows mark summer monsoon wind direction. Color shading on land represent rainfall mm/hour during summer monsoon.
- Figure 2:** Temporal variation in a) $\delta^{18}\text{O}_{\text{ruber}}$, b) *G. bulloides* relative abundance (%), c) Organic carbon ($\%C_{\text{org}}$), d) *G. ruber* Ba/Ca and e) *G. ruber* Mg/Ca-SST during the Termination-I (8-24 kyr BP) in core SSD004 GC03 collected from the northern tropical Indian Ocean. Inverted triangles indicate radiocarbon dated intervals. The shaded vertical bars represent Heinrich Stadial 1 (HS1), Bølling-Allerød (B-A) and Younger Dryas (YD).
- Figure 3:** A comparison of the SSD004 GC03 sea surface temperature data with other high resolution regional Mg-Ca SST records. ADM-159 (Liu et al., 2021); SO189-39KL (Mohtadi et al., 2014); SK218-1, (Govil and Naidu, 2011); SK17 (Anand et al., 2008); SK237 GC04 (Saraswat et al., 2013). The shaded vertical bars represent the Last Glacial Maximum (LGM); Heinrich Stadial 1 (HS1), Bølling-Allerød (B-A) and Younger Dryas (YD).
- Figure 4:** A comparison of the SSD004 GC03 regional precipitation-evaporation-runoff ($\delta^{18}\text{O}_{\text{sw-ivc}}$) data with other high resolution regional paleomonsoon records. SK237 GC04, $\delta^{18}\text{O}_{\text{sw-ivc}}$ (Saraswat et al., 2013); SO189-39KL, $\delta^{18}\text{O}_{\text{sw-ivc}}$ (Mohtadi et al., 2014); SK218-1, $\delta^{18}\text{O}_{\text{sw-ivc}}$ (Govil and Naidu 2011); MWS-1, Mawmluh Cave speleothem $\delta^{18}\text{O}$, Meghalaya, India (Dutt et al., 2015); ZS-10, Lugu Lake leaf wax hydrogen isotope, China (Zhao et al., 2021). The shaded vertical bars represent the Last Glacial Maximum (LGM); Heinrich Stadial 1 (HS1), Bølling-Allerød (B-A) and Younger Dryas (YD).
- Figure 5:** Temporal variation in a) Ba/Ca, b) temperature and ice volume corrected seawater $\delta^{18}\text{O}$ ($\delta^{18}\text{O}_{\text{sw-ivc}}$), c) relative abundance of *Globigerina bulloides*, d) organic carbon ($\%C_{\text{org}}$), e) Mg/Ca derived-SST during the glacial termination (8-24 kyr BP; grey line represents 3-points moving average) in the core SSD004 GC03 collected from the tropical Indian Ocean. Atmospheric carbon dioxide (CO_2) at EPICA Dome C, Antarctica (f; Parrenin et al., 2013), local $p\text{CO}_2$ (μatm) evolution in the tropical Indian Ocean (g; Naik et al., 2015), 21 July Boreal summer insolation at 7°N (h; Laskar et al., 2004), ΔT = northern and Southern Hemisphere thermal difference (i; Shakun et al., 2012) and Sedimentary $^{231}\text{Pa}/^{230}\text{Th}$ from the core GGC5 (j; McManus et al., 2004), Relative Sea Level/Ice-volume change (k; RSL in meters; Grant et al., 2012) are shown for comparison. Vertical bars: YD: Younger Dryas, B-A: Bølling-Allerød, HS1: Heinrich Stadial 1 and yellow bar is the interval (18.2-19.9 kyr BP) of warming prior to the global termination I. Inverted triangles indicate radiocarbon dated intervals.
- Figure 6:** The schematic diagram represents positive and negative climate feedback mechanism of the northern tropical Indian Ocean (NTIO) warming. Green and black arrow represent positive and negative feedback respectively. Dashed arrows represent atmospheric connection and solid arrows mark oceanic connection. The color shadings are the Indian Ocean warming-related SST anomalies from Hu and Fedorov (2019).

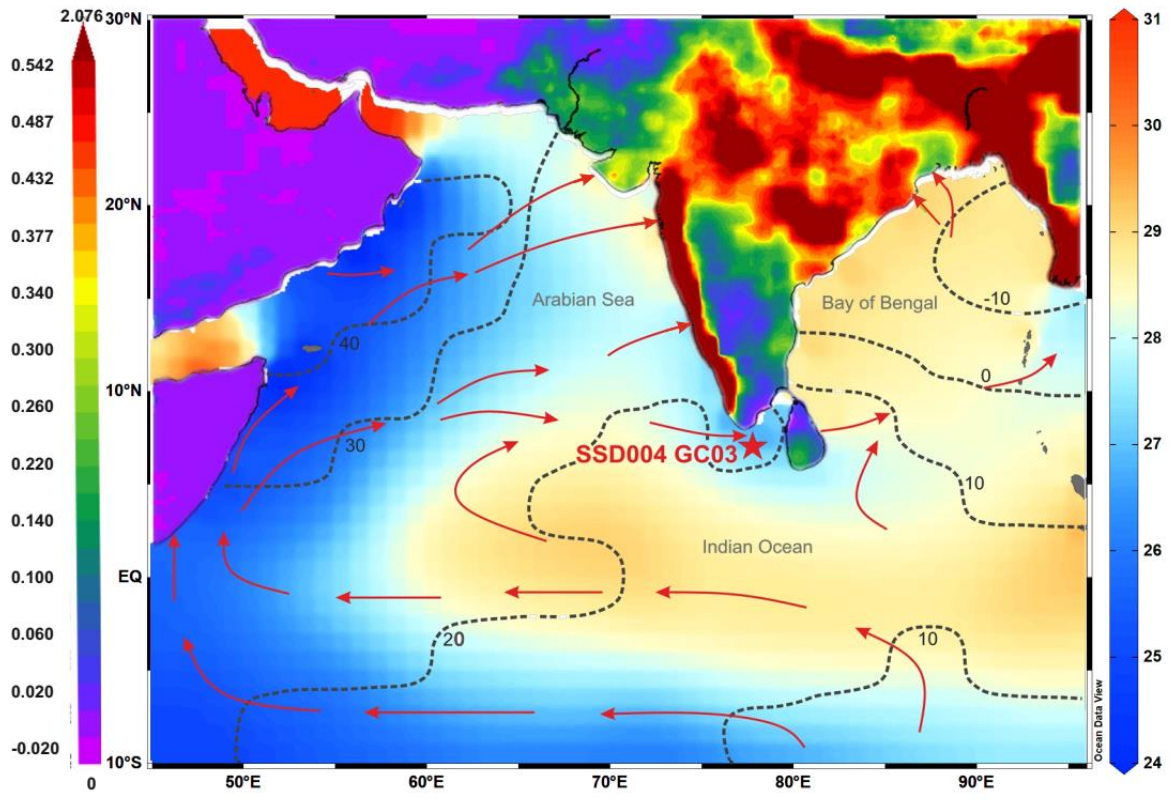


Figure 1

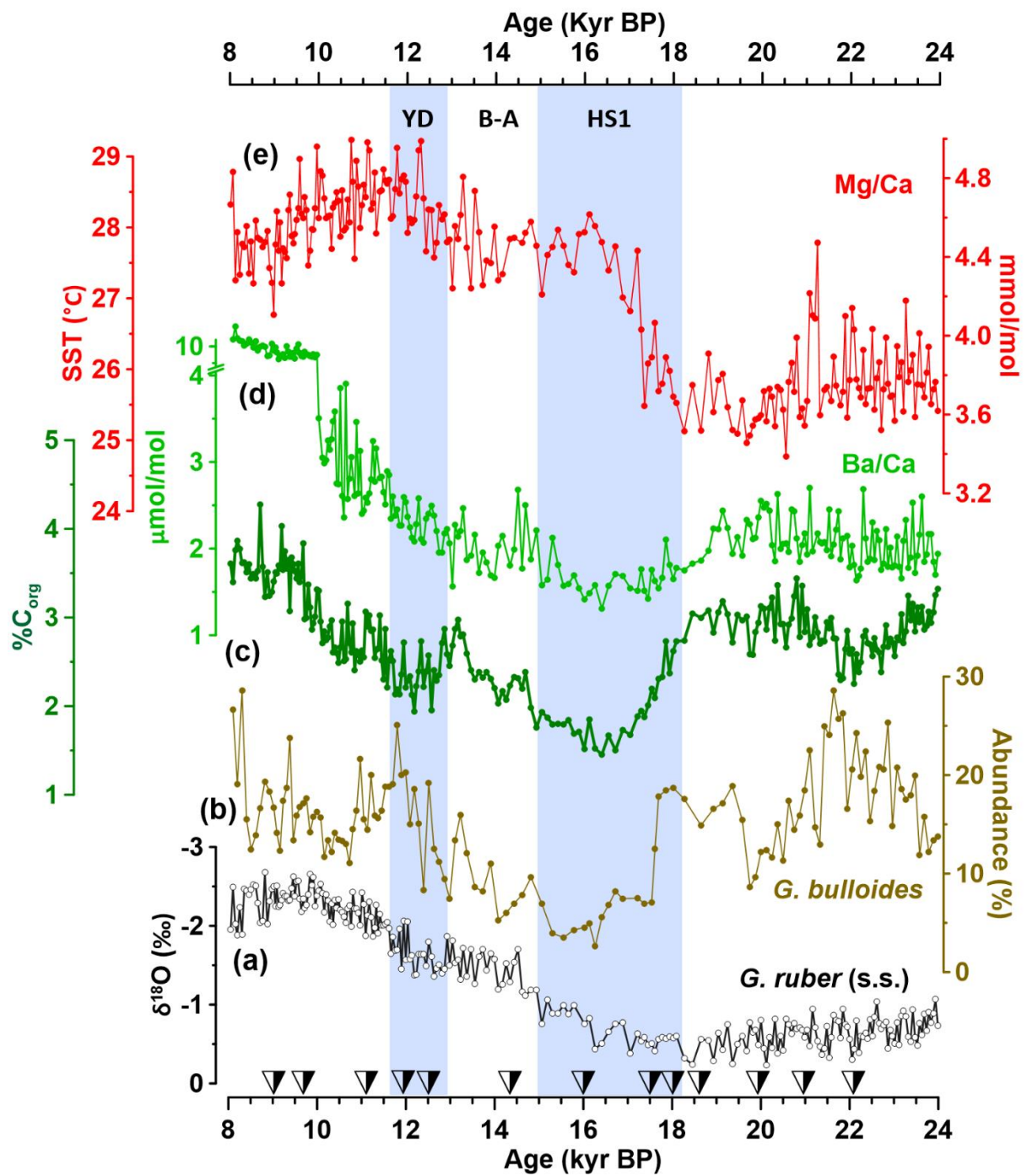


Figure 2

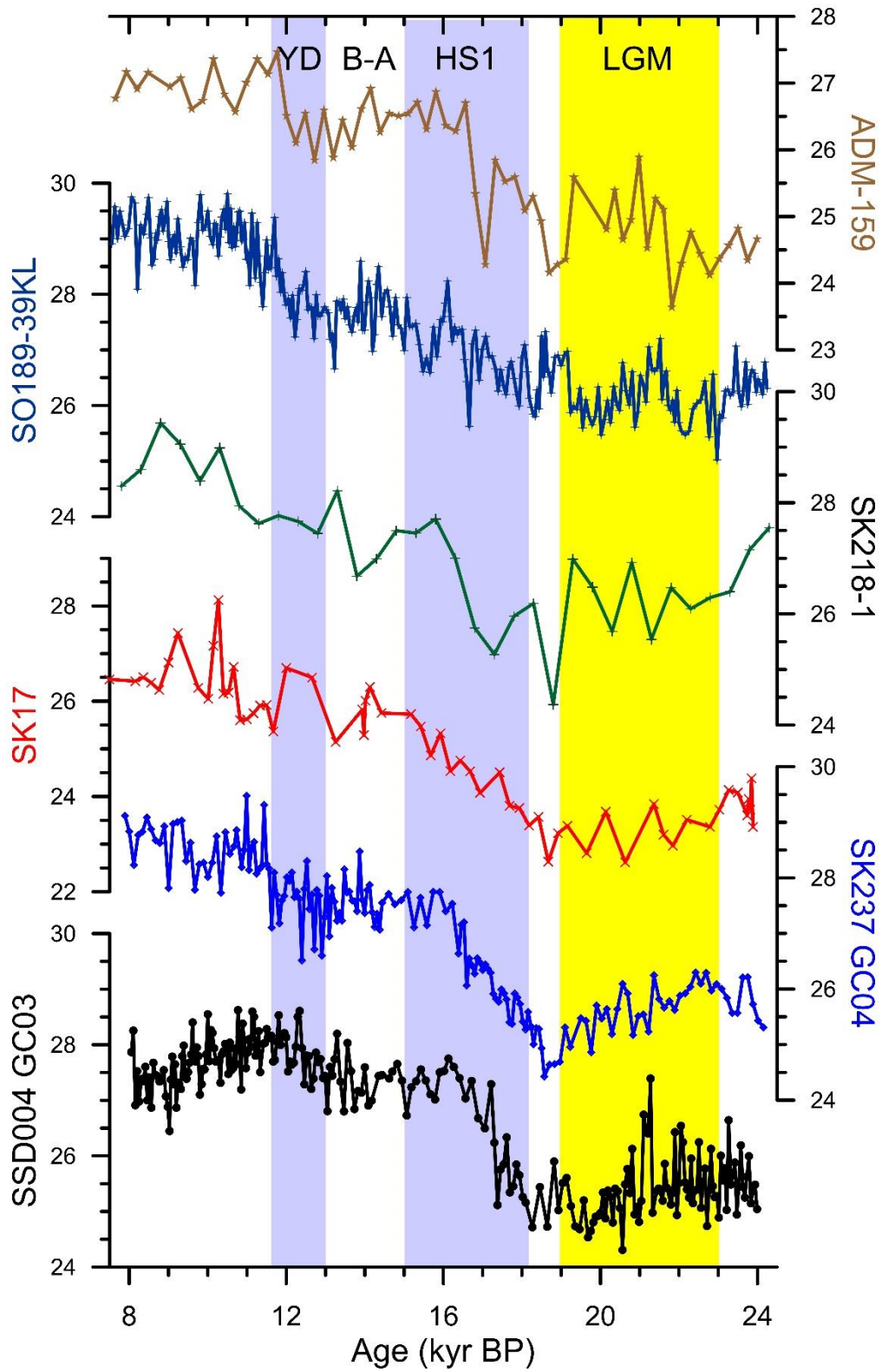


Figure 3

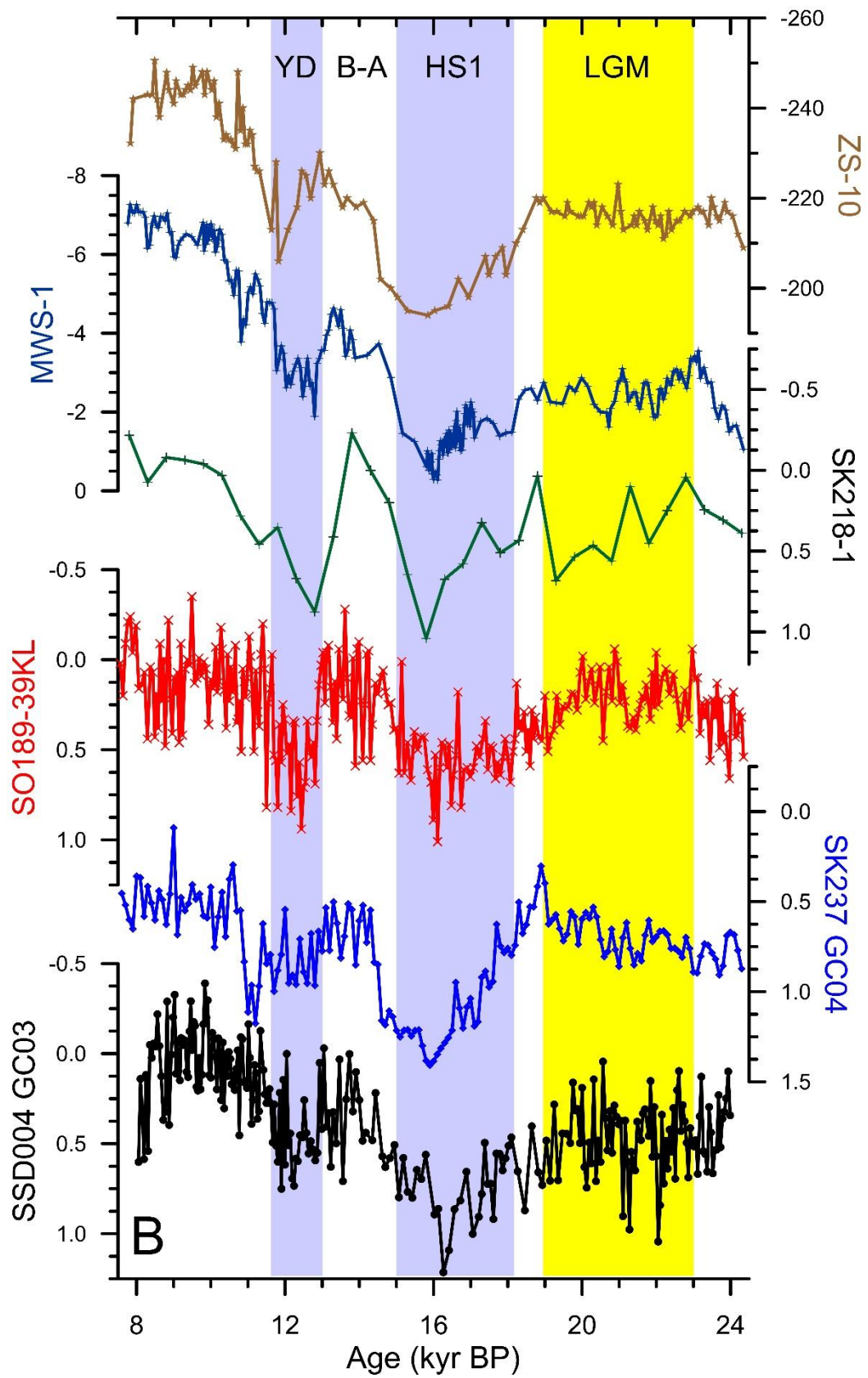


Figure 4

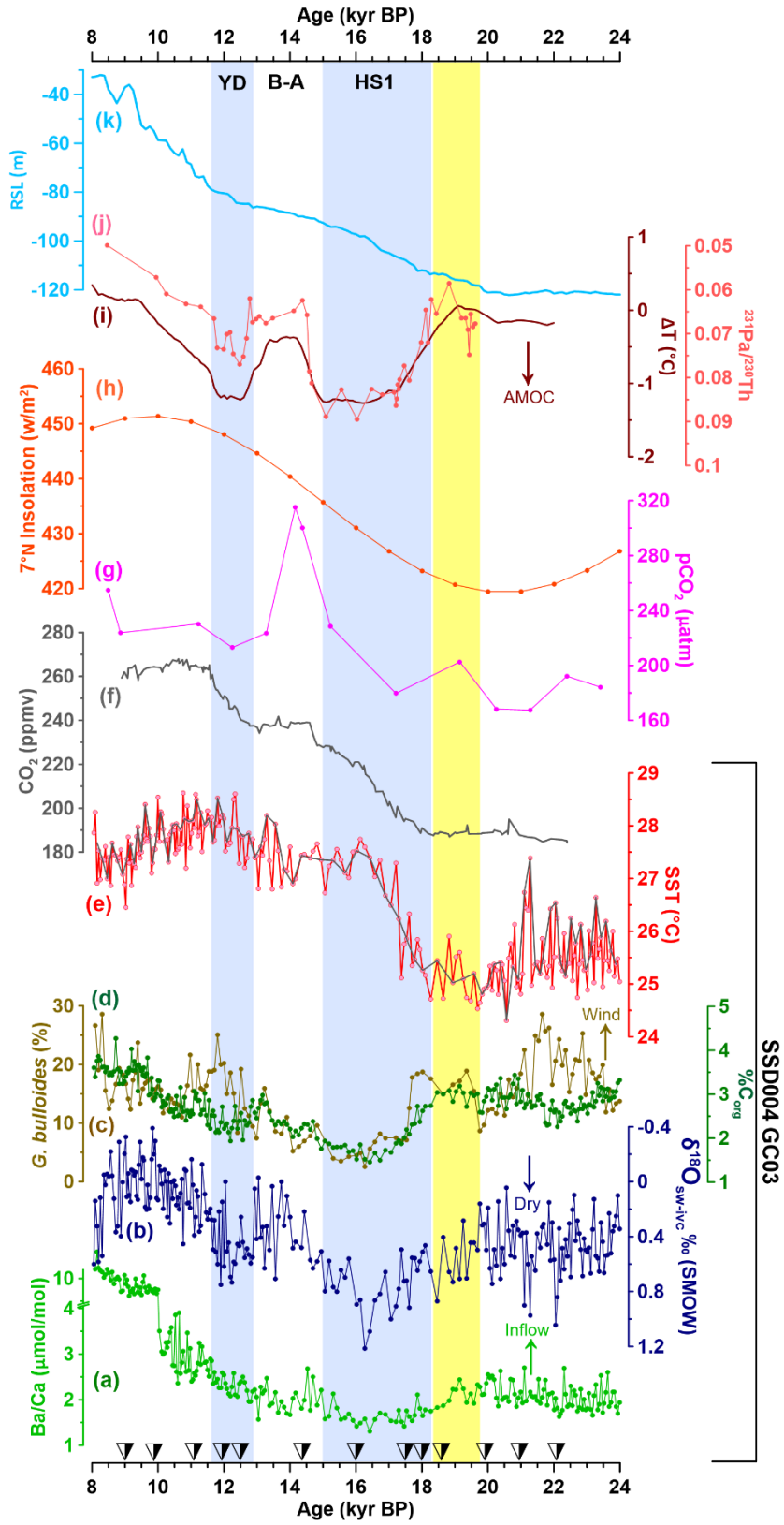


Figure 5

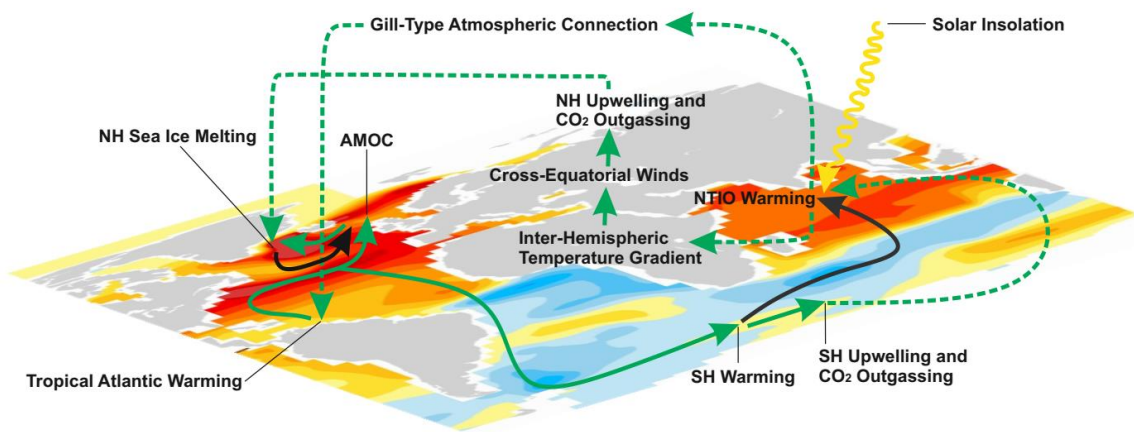


Figure 6

Table 1: Details of the accelerator mass spectrometer radiocarbon ages in core SSD004 GC03.

Lab ID	Core Depth (cm)	Foraminifera Species	¹⁴ C Age (yr)	Error (+/- yr)	Age Range (Cal. yr BP) (1σ)	Median Age (Cal. yr BP)
IUACD#20C3149	162.5	<i>G.ruber + T. sacculifer</i>	8481	38	8935 - 9126	9028
IUACD#20C3150	184.5	<i>G.ruber + T. sacculifer</i>	9119	45	9662 - 9907	9792
IUACD#20C3151	229.5	<i>G.ruber + T. sacculifer</i>	10171	47	11142 - 11322	11235
IUACD#19C2586	243.5	<i>G. ruber + T. sacculifer</i>	10748	55	11246-12183	11929
IUACD#19C2587	259.5	<i>G. ruber + T. sacculifer</i>	11040	80	12281-12912	12588
IUACD#19C2588	275.5	<i>G. ruber + T. sacculifer</i>	12799	51	13733-14789	14345
IUACD#19C2596		<i>C. wuellerstorfi + C. pachyderma</i>	13525	54	15583-15816	15693
IUACD#19C2589	287.5	<i>G. ruber + T. sacculifer</i>	13805	55	15452-16313	16022
IUACD#19C2590	294.5	<i>G. ruber + T. sacculifer</i>	14962	58	16506-17592	17567
IUACD#19C2591	305.5	<i>G. ruber + T. sacculifer</i>	15003	72	17226-18605	18097
IUACD#19C2592	309.5	<i>G. ruber + T. sacculifer</i>	16061	78	18118-18844	18670
IUACD#19C2593	317.5	<i>G. ruber + T. sacculifer</i>	17078	71	19396-20248	19958
IUACD#19C2597		<i>C. wuellerstorfi + C. pachyderma</i>	17357	73	20292-20523	20403
IUACD#19C2594	335.5	<i>G. ruber + T. sacculifer</i>	17700	71	20430-21440	20951
IUACD#19C2595	343.5	<i>G. ruber + T. sacculifer</i>	18937	78	21598-22313	22189